This paper has been accepted for publication in Composite Structures.

Predicting notched tensile strength of full-scale composite structures from small coupons using fracture mechanics

Xiaodong Xu[a*], Shin-ichi Takeda[b], Yuichiro Aoki[b], Stephen R. Hallett[a] and Michael R. Wisnom[a]

[a]Bristol Composites Institute (ACCIS), University of Bristol, United Kingdom

[b]Structures and Advanced Composite Research Unit, Japan Aerospace Exploration Agency (JAXA), Japan

Abstract: *The initial fracture propagation within a full-scale stiffened quasi-isotropic composite panel and coupons with stringer feet under tensile loads was investigated. The specimens were made from Non-Crimp Fabric through Vacuum assisted Resin Transfer Moulding. The failure loads of all configurations were successfully related using the same value of trans-laminar fracture energy. The method involved independent tests of scaled-down Over-height Compact Tension specimens and the Virtual Crack Closure Technique. It was found to be crucial to include the fully developed damage process zone in the crack length and to interpret the results carefully in order to identify the failure loads consistently.*

Keywords: Fracture mechanics; Notch; Virtual Crack Closure Technique (VCCT); Vacuum assisted Resin Transfer Moulding (VaRTM); Non-Crimp Fabric (NCF).

* Corresponding author Tel.: +44 (0)117 33 15098
E-mail address: xiaodong.xu@bristol.ac.uk (X. Xu)

1. Introduction

Large composite structures have become widely used in the aerospace industry. Notched strength is a design driver for these composite structures. To assess the structural integrity of large notched structures, full-scale notched composite panels are normally tested. For example, Boeing and the National Aeronautics and Space Administration (NASA) joined forces to address the issues associated with transport aircraft pressurised fuselage damage tolerance in the 1990s [1]. Walker et al. [1] found that the models based on Linear Elastic Fracture Mechanics (LEFM) were inaccurate for predicting the large notch strengths of four laminate combinations tested, except for one IM7/8551-7 laminate, loaded in its stiffer direction. Even in this exceptional case, the classical fracture mechanics models needed to be calibrated through a 2.5 in. notch (63.5 mm). Consequently, strain-softening models calibrated through small-scale specimens instead of fracture mechanics models were proposed for two full-scale stiffened panels. More recently, a stiffened composite panel test was carried out at the Japanese Aerospace Exploration Agency (JAXA) [2]. The purpose of the test was to investigate the trans-laminar fracture propagation in the full-scale stiffened panel. Progressive failure analysis based on Hashin's failure criteria and cohesive zone model was unsuccessful in quantitatively correlating with the experiments. A series of much smaller centre-notched coupons with stringer feet, made of the same material, were also tested. A second attempt was made to predict the failure of the full-scale stiffened panel with data from the small stiffened coupons with some success [3]. However, it was required to make assumptions about the size of the damage process zone. Another example of large scale testing is a full-scale Pultruded Rod Stitched Efficient Unitized Structure (PRSEUS) fuselage panel experimentally investigated under a joint program

conducted by NASA, the Federal Aviation Administration (FAA), and the Boeing Company. The test results demonstrated that the PRSEUS design shows improved damage-containment capability [4]. A progressive failure analysis of the PRSEUS fuselage structure was later conducted by representing the trans-laminar fracture with a through-the-thickness cohesive crack, in which the interaction of damage propagation in the skin with delamination of the stiffener was also considered [5]. Because of the difficulty in predicting failure of full-scale stiffened composite structures, many studies have been conducted on scaled un-stiffened notched specimens. For example, Gonzáles and Knauss conducted large compact tension tests with notch lengths of up to 200 mm [6]. Xu et al. investigated into the size effects in large centre-notched specimens with up to a 50.8 mm notch length [7]. Salviato et al. tested edge notched specimens with a notch length of up to 16 mm [8]. These studies of large notched coupons [6-8] demonstrate a fracture mechanics scaling at large notch lengths, but fracture mechanics does not apply to small notches [7]. How to relate un-stiffened laboratory coupons to full-scale stiffened composite panels is still not clear. In this paper, the applicability of fracture mechanics for the strength prediction of full-scale stiffened panels based on small scale coupon tests is investigated.

The Over-height Compact Tension (OCT) test was developed from the traditional compact tension test [9] to determine fracture properties of composite laminates [10]. Challenges arise in conducting these fracture tests such as the measurement of crack lengths [11, 12], but they remain an effective method for the determination of the trans-laminar fracture energy and R-curve [13, 14]. Standard OCT specimens may suffer from buckling at the rear end, so anti-buckling guides are often needed. A scaled-down OCT test can however reduce the risk of buckling while still being able to capture the fully

developed damage process zone for initial fracture propagation [15]. In the current paper, a scaled-down OCT test is conducted to independently determine the trans-laminar fracture energy for initial fracture propagation and the size of the fully developed damage process zone. It is shown that the trans-laminar fracture toughness measured from the small-scale OCT test can be related to that of the full-scale stiffened panel for initial fracture propagation.

The Virtual Crack Closure Technique (VCCT) is often used to determine the strain energy release rate (G) for intra-laminar and inter-laminar matrix cracking in composite laminates [16-18]. The critical strain energy release rate, known as the fracture energy (G_C), is often regarded as a material property. One limitation of this VCCT approach is that it ignores the non-linear material response introduced by the damage process zone ahead of the notch tip. The limitation can be overcome by introducing a strain-softening material response [1, 19, 20]. However, extracting an objective constitutive law for trans-laminar fracture itself requires special procedures [12, 21]. In the current study, the notch length of 200 mm in the full-scale stiffened panel is long compared with the damage zone, so LEFM can be applicable. VCCT was adopted as a numerical tool for the determination of the strain energy release rate for trans-laminar fracture propagation in the stiffened panel. VCCT was also applied to the OCT specimens and the stiffened coupons for consistency. In these cases, the notch lengths are from 70 mm down to about 17 mm, so some adjustments to LEFM may be necessary as the damage process zone may be significant compared to the shorter notch lengths. The effect of the damage process zone on G when applying VCCT was therefore considered. In Ref. [15], it has been demonstrated that the fully-developed damage process zone size and trans-laminar fracture energy for initial fracture

propagation in three different sized OCT specimens of the same material (IM7/8552 carbon/epoxy prepreg) and the same quasi-isotropic stacking sequence are approximately the same. The size of the fully-developed damage process zone is also similar between the scaled OCT specimens [15] and large centre notched specimens [7]. It is therefore assumed that the fully-developed damage process zone size and the trans-laminar fracture energy for initial fracture propagation are constant for the current material and quasi-isotropic stacking sequence. It was found that if the damage process zone is considered, the G_C back-calculated from different sized specimens and the full-size panel can be related.

Following the test programme at JAXA [2], it was considered how to relate the full-scale stiffened panel to the coupons with stringer feet [3]. Fracture mechanics was found to be a promising tool for the failure predictions if the size of the damage process zone is taken into account. However, the size of the zone was not known and so an estimate was used in the previous analyses. In the current study, the size of the damage process zone was firstly measured in independent scaled-down OCT tests. The strain energy release rate against crack length curves at the experimental failure loads were obtained via VCCT analyses of the scaled-down OCT tests (16.5 mm notch length), small coupons with stringer feet (17.5 mm and 70 mm notch lengths) and the full-scale stiffened panel (200 mm notch length). The energy release rates from all four tests crossed at a short crack length. This point represents the trans-laminar fracture energy for initial fracture propagation of the laminate. It also corresponds to a crack length equivalent to the fully-developed damage process zone, and the length agrees with the independently measured damage process zone size. Finally, the failure of the full-scale stiffened panel and small coupons with string feet can be related. This has not been

achieved previously in the literature covering such a wide range of notch lengths from about 17 mm to up to 200 mm, and demonstrates how small scale coupons can be successfully used to predict large scale structural response.

2. Material processing

All composite laminates used in the current study were from the same panel manufactured at JAXA though Vacuum assisted Resin Transfer Moulding (VaRTM), one of the low-cost composite integral moulding methods. The material used was biaxial carbon Non-Crimp Fabric (NCF) made from STS-24k fibres by SAERTEX Co. KG, and epoxy resin XNR6809/XNH6809 by Nagase Chemtex Co. The layup used in all configurations was $[(45/-45)/(0/90)]_{2S}$. The nominal laminate thickness was 2 mm except for the end of the foot of the hat-shaped stringers, which was tapered. The actual thickness of the cured plates varied slightly at different locations, with an average value of 2.18 mm. The nominal thickness was used for all analyses for consistency.

3. Damage process zone

3.1 Scaled-down OCT tests

OCT tests were conducted to extract the size of the fully developed damage process zone and the trans-laminar fracture energy. The material, the stacking sequence and notch orientation were kept the same as those for the stiffened panel and coupons, so the measured damage process zone and the trans-laminar fracture energy from the OCT tests are representative. Because the thickness of the current NCF laminates is about 2 mm, a scaled-down version of the standard OCT specimen [10] was used to avoid potential buckling at the rear end of the specimen as shown in Figure 1. The notch is 1 mm wide with a 0.5 mm radius tip. It has already been shown that the scaled-down

OCT specimen and the standard OCT specimen yield the same trans-laminar fracture energy and fully-developed damage process zone size for initial fracture propagation [15]. Initial fracture propagation is defined as the starting point of a growing crack, where all plies are already broken. Damage before this point, where there are still intact fibres, is considered to be the growth of a damage process zone, which is not yet fully developed. After initial propagation, it is possible that the damage zone may grow further, giving rise to an R-curve with increasing fracture energy, but this is not considered in the current paper.

Five identical specimens were tested. Their load – Pin Opening Displacement (POD) relationships are shown in Figure 2. Test 1 was conducted until ultimate failure. Test 2 was interrupted early on at the very first small load drop. Test 3 was stopped after the peak load. Test 4 was interrupted later, before ultimate failure. Test 5 was stopped just before the peak load. As a result, there were three specimens tested (Tests 1, 3 and 4) for the calculation of the average peak load. In Figure 2, the curves are fairly linear at the beginning, and then become slightly non-linear with the presence of some small load drops. There are several large load drops after the peak. The specimens recover, and then fail catastrophically. No buckling was observed during the tests, and the ultimate failure was due to compressive failure at the rear end of the specimen. The specimens from the interrupted tests (Tests 3, 4 and 5) were prepared for X-ray Computed Tomography (CT) scanning to study the development of internal damage at the notch tip before and after the peak load. A small initial force of 140 N existed in Test 5 before loading, but this is too low to affect the formation of the damage process zone. The samples for CT scanning were soaked in a bath of zinc iodide penetrant to enhance contrast. A Nikon XT H 225ST CT scanner was used, which has proprietary

225 kV microfocus X-ray source offering a 3 μm focal spot size.

3.2 Fully developed damage process zone

The CT scan images taken after the peak load from Test 3 in Figure 3 show that fibres are broken in all the plies. One matrix split appears in the 90° plies. The black marks are believed to be voids near the fibre tows due to the VaRTM processing. In contrast, the CT scan images taken before the peak load from Test 5 show that fibres are only broken in some of the 0° plies, but are still intact in the ±45° plies as shown in Figure 4. Matrix cracks can also be seen in the 90° plies before the peak load. It was previously considered that the damage process zone is only fully developed when all plies are broken [15], which occurred after the peak load in the current tests. The CT scan images taken further into the stable fracture propagation before the ultimate failure from Test 4 in Figure 5 illustrate that the through-thickness crack grows in a self-similar manner during the stable fracture propagation. Meanwhile, the applied load recovers after the peak load, which implies that there exists an R-curve.

In the CT scan images, there is a clear pattern showing that the fibre breakage arrests near the adjacent tow, which limits the extent of fibre breakage in each ply. Because the NCF fabrics were not exactly aligned according to the positions of their 0° tows (along the loading direction), the fibre breakage length from the notch is slightly different in each ply. The fibre breakage length is affected by the relative position between the notch tip and the 0° tows, which is different from laminates composed of unidirectional prepregs, which are more uniform. The damage near the surfaces is slightly greater than within the interior plies due to delaminations. The fibre breakage lengths in all 0° and ±45° plies after the peak load but before crack propagation were measured to quantify the size of the damage process zone, with an average size of 3.1

mm (C.V. 18 %). This value is close to the reported value of 2.5 mm for IM7/8552 carbon/epoxy laminates [15]. According to the definition in Ref. [15], the trans-laminar fracture energy for initial fracture propagation is the value measured when the damage process zone is fully developed. It was found to be a constant value for initial fracture propagation, before which the damage process zone is still developing.

4. Stiffened panel and coupon tests

4.1 Experimental configurations

The stiffened panel is 900 mm × 750 mm with three hat-shaped stringers co-cured to the skin as shown in Figure 6. The end of the stringer foot was tapered over 10 mm down to zero. A 200 mm centre notch was introduced to the panel by using a saw. The notch is 4 mm wide with a rectangular shaped tip. The tensile load was applied by an Instron 2500 kN hydraulic-driven test machine under displacement control at a rate of 0.5 mm/min. Steel fixtures were fitted to both ends of the panel. A total of 60 electrical strain gauges and 6 acoustic emission sensors were attached on the surface of the panel. The strain gauges had a 2.8 mm wide base. Their centroid locations across the specimen width are illustrated in Figure 7. When damage and fracture grow in the stiffened panel, the strains should change. The strain gauges can therefore be used as crack detectors.

The small coupons were manufactured in the same way as the full-scale stiffened panel. The mechanical properties and thickness of the coupon therefore should also be the same as those of the stiffened panel. The coupons are 300 mm × 210 mm with a stringer foot the same as that in the full-scale panel co-cured to each long edge as shown in Figure 8. The end of the stringer foot was tapered over 10 mm down to zero. 2 mm-wide central notches with 1 mm radius at the tips were introduced to the coupons by machining. The lengths of the two centre notches are 17.5 mm and 70 mm. The tensile

load was applied by the same Instron 2500 kN hydraulic-driven test machine under displacement control at a rate of 0.5 mm/min. Thick glass fibre reinforced polymer end tabs were attached to both ends of the coupon so as to fit into the grips. A total of 6 electrical strain gauges which have a 2.8 mm wide base were attached on the surface. Their centroid locations across the specimen width are illustrated in Figure 9.

4.2 Full-scale stiffened panel test results

It is crucial to determine the failure load for initial fracture propagation in the large stiffened panel test. This was indicated by the failure of the strain gauges close to the notch tips in the present test. However, it has already been identified that the size of the fully developed damage process zone of the current material is 3.1 mm on average. It is therefore expected that the strain gauges S1 and S8 which are 1.5 mm away from the notch tips will fail during development of the damage process zone and will therefore not give an indication of fracture propagation. The failure of the S2 and S9 gauges, which are 5 mm away from the notch tips, should be representative of initial fracture propagation. This is because the average size of the fully developed damage process zone is close to the edges of the 5 mm strain gauges, which are 3.6 mm away from the notch tips.

Table 1 summarises the failure sequence of the strain gauges and the corresponding loads from Figure 10. The failure of the strain gauges nearer to the notch usually affects the reading of the gauge next to it which typically fails at a slightly higher load. However, S2 gauge (5 mm) and S1 gauge (1.5 mm) failed almost at the same time at 182 kN, which might be due to the fact that they were bonded together. At 235 kN, S9 gauge (5 mm) failed and there are substantial changes in the next gauges

S10 and S11, indicating a significant event. The experimental failure load for initial fracture propagation is therefore taken to be 235 kN, and the damage process zone is expected to be fully developed. Beyond this point, the panel saw a short period of stable fracture propagation until the maximum load. After the peak load was reached, the crack almost reached both stringers. The failure and debonding of the stringers occurred thereafter, consideration of which is beyond the scope of the current study.

4.3 Stiffened coupon test results

It is also crucial to determine the experimental loads for initial fracture propagation in the coupon tests. Similar to the full-scale stiffened panel, the failure of the nearest strain gauges to the notch tip occurs during the formation of a fully developed damage process zone. The failure of ST5 gauge which is 5 mm away from the notch tips should therefore be representative of initial fracture propagation.

As shown in Figure 11 (a), at 143 kN, ST5 gauge (5 mm) failed in the short-notch coupon. As a result, the experimental failure load for initial fracture propagation in the short-notch coupon is taken to be 143 kN, when the damage process zone is expected to be fully developed. In Figure 11 (b), at 88 kN ST5 gauge (5 mm) failed in the long-notch coupon, which is taken as the experimental failure load for initial fracture propagation. It also seems that fracture grows stably until 93.6 kN, which implies the existence of an R-curve.

5. Determination of strain energy release rates

5.1 Virtual Crack Closure Technique

VCCT has been applied to all of the cases in the linear elastic finite element software MSC Nastran. As an example, the scaled-down OCT specimen is shown in

Figure 12. Half of the height of the scaled-down OCT specimen was modelled. One 8-node solid element through the thickness of the specimen (2 mm) was used with homogenised isotropic material properties as shown in Table 2. The mesh was refined along the crack path (0.3 mm element edge length). Symmetry boundary conditions were applied to the nodes at the boundaries. Multi-Point Constraint (MPC) equations link the nodes as a rigid body where the load was applied. The notch was represented by an infinitely sharp crack at the symmetry plane perpendicular to the loading direction.

The strain energy release rate G is calculated in a two-step VCCT analysis according to Ref. [18]. Linear elastic FE models of centre-notched specimens with different mesh sizes (coarse 1 mm, normal 0.5 mm and fine 0.1 mm), different notch tip radii and of the same material properties (Table 2) were established previously [3]. It was demonstrated that the Stress Intensity Factor (SIF) values through VCCT analyses are not sensitive to mesh size with this level of refinement and infinitely sharp cracks. Although the initial values are different, the SIF values for different blunt notches (1 mm, 2 mm, 4 mm radius and 4 mm wide rectangular notch tips) converge to those for infinitely sharp notches quickly from 2 mm crack growth. Therefore, infinitely sharp notches were used to calculate energy release rates for the real notches in the current study.

5.2 Analysis results

Strain energy release rates are plotted against crack extension in Figure 13 for all four cases using the experimental failure loads (235 kN for stiffened panel, 143 kN for 17.5 mm notched coupon, 88 kN for 70 mm notched coupon and 2.54 kN for the OCT specimen) at which the strain gauges 5 mm away from the notch tips fail. The effect of

the damage process zone on *G* can be accounted for as equivalent to an additional crack length being added to the initial crack length. *G* values of the four configurations are all similar at about 3 mm crack length, which is the same as the size of the fully developed damage process zone measured from the CT scans. This is consistent with a constant trans-laminar fracture energy for initial crack propagation of approximately 85 kJ/m^2 as shown in Figure 13.

It is crucial to use the appropriate failure loads that represent the initial fracture propagation. For example, if the failure loads (181 kN for stiffened panel, 108 kN for 17.5 mm notched coupon and 61 kN for 70 mm notched coupon) are taken according to the readings of the strain gauges closest to the notch tips (1.5 mm), there is a large discrepancy between the *G* values of the four configurations, as shown in Figure 14. It is not possible to relate all the cases even if the size of the fully developed damage process zone is considered. This highlights the necessity of both considering the effect of the damage process zone and selecting the appropriate failure loads.

6. Discussion

In the current paper, the full-scale stiffened panel has a long notch of 200 mm. The measured average size of the fully-developed damage process zone in the scaled-down OCT specimens is 3.1 mm, which is relatively small-scale compared to the notch length. Consequently, LEFM is applicable for the stiffened panel. The OCT specimens and the stiffened coupon with a short notch have a notch length of about 17 mm, so some adjustments to LEFM are necessary.

In order to predict failure of future full-scale stiffened panels under tensile loads, two key findings of the current study should be taken into account. Firstly, the size of

the fully developed damage process zone should be carefully determined with small coupon made of the same material and stacking sequence, and added to the initial crack length when calculating the strain energy release rates. For example, the measured size of the fully developed damage process zone for the current material was found to be 3.1 mm, which was then added to the initial crack length in the VCCT analyses. This type of adjustment to LEFM by adding a crack-tip damage process zone is a common approach for composites [22, 23]. The influence of the adjustment on trans-laminar fracture energy will be greater for short cracks than for long cracks [23]. Secondly, appropriate loads should be used representing initial fracture propagation in small coupon tests when determining the trans-laminar fracture energy. For example, failure of strain gauges was used to indicate the location of the crack front in the current study and hence to determine the load at which fracture propagation started. Finally, the critical strain energy release rate can be determined from VCCT analysis of scaled-down OCT specimens that include the damage process zone length in the initial crack length. This can then be used to derive the failure load for the full-scale stiffened panel based on VCCT analysis that also includes the damage process zone length. The current approach is computationally cost-efficient, and is suitable for the fracture analysis of full-scale structures if the damage process zone is already determined.

There is clear evidence that an R-curve exists in the current material, shown by the stable fracture propagation in all configurations. Due to limited information from the full-scale panel test and the stiffened coupon tests, the full R-curve determination is beyond the scope of this paper. The current study focuses on the trans-laminar fracture energy for initial fracture propagation, namely, the starting point on the R-curve. The full R-curve will be characterized in the future. Without considering the R-curve, the

entire fracture propagation in the stiffened coupons and panel cannot be described. However, by using the trans-laminar fracture energy for initial fracture propagation, the failure prediction for the full-scale stiffened panel will be conservative.

7. Conclusions

An approach to relate the initial fracture propagation of full-scale stiffened composite panels to that of small stiffened coupons and scaled-down Over-height Compact Tension (OCT) specimens under tensile loads has been successfully demonstrated. The important implication for engineering applications is that linear elastic fracture mechanics can be applied to the failure prediction of full-scale notched stiffened panels with long notches provided the damage process zone is taken into account.

The critical strain energy release rate, i.e. trans-laminar fracture energy is the key link, bridging the dimension gap between the scaled-down OCT specimen, the small stiffened coupons and the full-scale stiffened panel. The size of the fully developed damage process zone, which was measured here in independent scaled-down OCT tests, should be included both in the determination of the trans-laminar fracture energy and in calculating the energy release rate to predict failure.

References

[1] Walker TH, Ilcewicz LB, Polland DR, Poe Jr. CC. Tension fracture of laminates for transport fuselage Part II: large notches. NASA/Boeing Advanced Technology Composite Aircraft Structures (ATCAS); 1995.

[2] Aoki Y, Takeda S, Shoji H, Sugimoto S, Iwahori Y. Evaluation on discrete source damages of CFRP stiffened panels. 28th International Congress of the Aeronautical

Sciences. Brisbane. 2012.

[3] Xu X, Takeda S, Hallett SR, Wisnom MR. On the application of fracture mechanics to a full-scale stiffened composite panel test. In: Hallett SR, Remmers JJC, editors. V ECCOMAS Thematic Conference on the Mechanical Response of Composites-COMPOSITES 2015. Bristol. 2015.

[4] Bergan A, Bakuckas Jr J, Awerbuch J, Tan T-M. Assessment of damage containment features of a full-scale PRSEUS fuselage panel. Composite Structures. 2014;113:174-85.

[5] Bergan AC, Dávila CG, Leone FA, Awerbuch J, Tan T-M. An analysis methodology to predict damage propagation in notched composite fuselage structures. SAMPE 2015 Baltimore, MD, USA. 2015.

[6] Gonzáles L, Knauss WG. Scaling global fracture behavior of structures-sized laminated composites. International Journal of Fracture. 2002;118:363-94.

[7] Xu X, Wisnom MR, Mahadik Y, Hallett SR. An experimental investigation into size effects in quasi-isotropic carbon/epoxy laminates with sharp and blunt notches. Composites Science and Technology. 2014;100:220-7.

[8] Salviato M, Kirane K, Esna Ashari S, Bažant ZP, Cusatis G. Experimental and numerical investigation of intra-laminar energy dissipation and size effect in two-dimensional textile composites. Composites Science and Technology. 2016;135:67-75.

[9] ASTM, Standard, E399-90. Standard test method for plane-strain fracture toughness of metallic materials. West Conshohocken, PA, USA: ASTM International; 1990 (1997).

[10] Kongshavn I, Poursartip A. Experimental investigation of a strain-softening approach to predicting failure in notched fibre-reinforced composite laminates.

Composites Science and Technology. 1999;59:29-40.

[11] Bergan A, Dávila C, Leone F, Awerbuch J, Tan T-M. A mode I cohesive law characterization procedure for through-the-thickness crack propagation in composite laminates. Composites Part B: Engineering. 2016;94:338-49.

[12] Zobeiry N, Vaziri R, Poursartip A. Characterization of strain-softening behavior and failure mechanisms of composites under tension and compression. Composites Part A: Applied Science and Manufacturing. 2015;68:29-41.

[13] Pinho ST, Robinson P, Iannucci L. Fracture toughness of the tensile and compressive fibre failure modes in laminated composites. Composites Science and Technology. 2006;66:2069-79.

[14] Camanho PP, Catalanotti G. On the relation between the mode I fracture toughness of a composite laminate and that of a 0° ply: Analytical model and experimental validation. Engineering Fracture Mechanics. 2011;78:2535-46.

[15] Xu X, Wisnom MR, Mahadik Y, Hallett SR. Scaling of fracture response in over-height compact tension tests. Composites Part A: Applied Science and Manufacturing. 2015;69:40-8.

[16] Rybicki EF, Schmueser DW, Fox J. An energy release rate approach for stable crack growth in free-edge delamination problem. Journal of Composite Materials. 1977;11:470-87.

[17] Jimenez MA, Miravete A. Application of finite-element method to predict the onset of delamination growth. Journal of Composite Materials. 2004;38:1309-35.

[18] Krueger R. Virtual crack closure technique: History, approach and applications. Applied Mechanics Reviews. 2004;57:109-43.

[19] Maimí P, González EV, Gascons N, Ripoll L. Size effect law and critical distance

theories to predict the nominal strength of quasibrittle structures. Applied Mechanics Reviews. 2013;65:020803--16.

[20] Goutianos S, Sørensen BF. The application of J integral to measure cohesive laws under large-scale yielding. Engineering Fracture Mechanics. 2016;155:145-65.

[21] Ortega A, Maimí P, González EV, Trias D. Characterization of the translaminar fracture Cohesive Law. Composites Part A: Applied Science and Manufacturing. 2016;91:501-9.

[22] Daniel IM. Strain and failure analysis of graphite/epoxy plates with cracks. Experimental Mechanics. 1978;18:246-52.

[23] Harris CE, Morris DH. Effect of laminate thickness and specimen configuration on the fracture of laminated composites. Composite Materials: Testing and Design (Seventh Conference). 1986;ASTM STP 893:117-95.

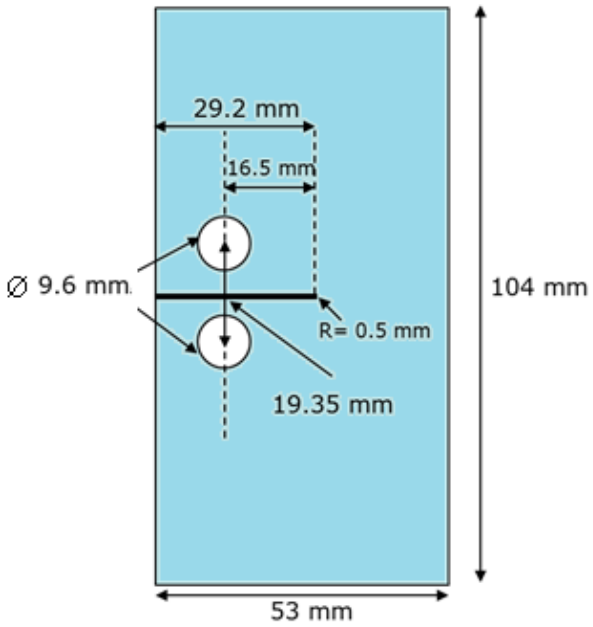

Figure 1. Scaled-down OCT specimen dimensions.

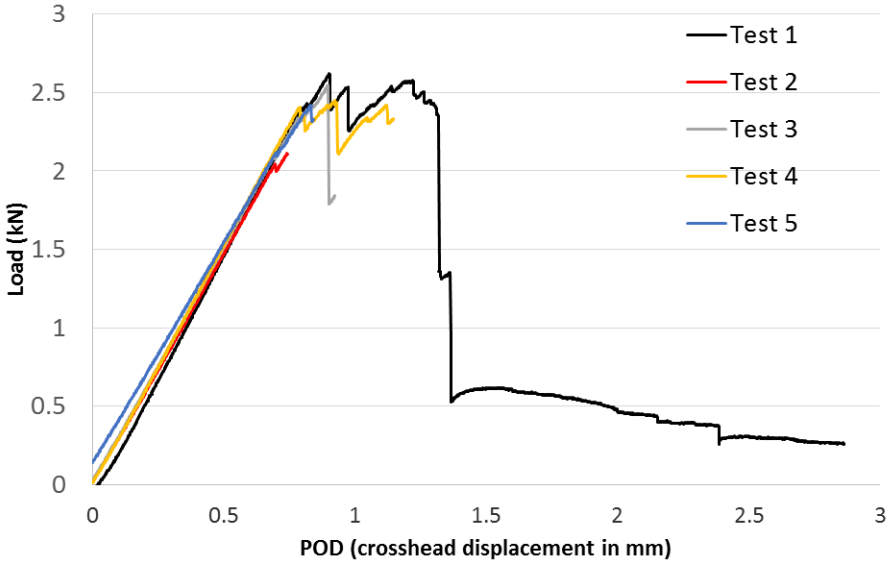

Figure 2. Load-POD curves from the scaled-down OCT tests.

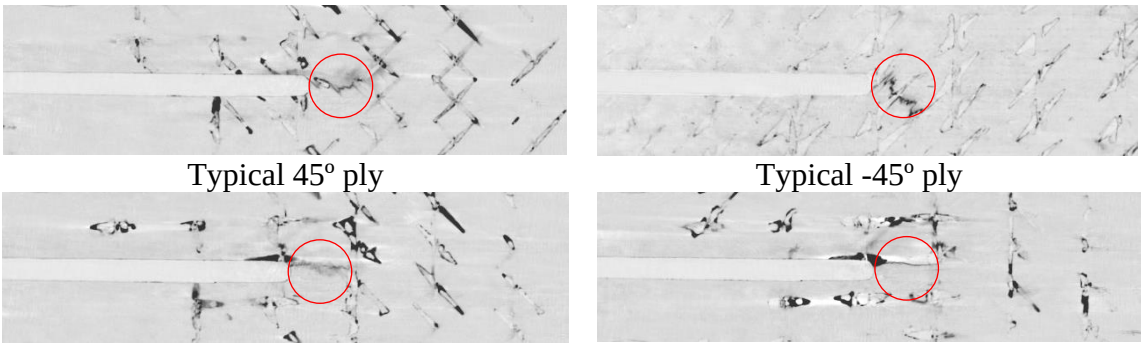

Typical 45º ply | Typical -45º ply

Typical 0º ply | Typical 90º ply

Figure 3. CT scan images of the damage process zone after the peak load from Test 3 (a red circle with a 3-mm diameter indicating the damage process zone).

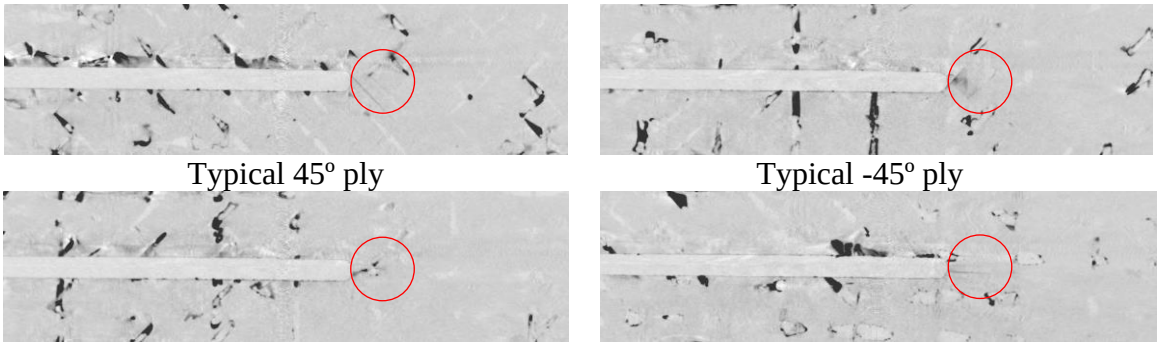

Figure 4. CT scan images of the damage process zone before the peak load from Test 5 (a red circle with a 3-mm diameter indicating the damage process zone).

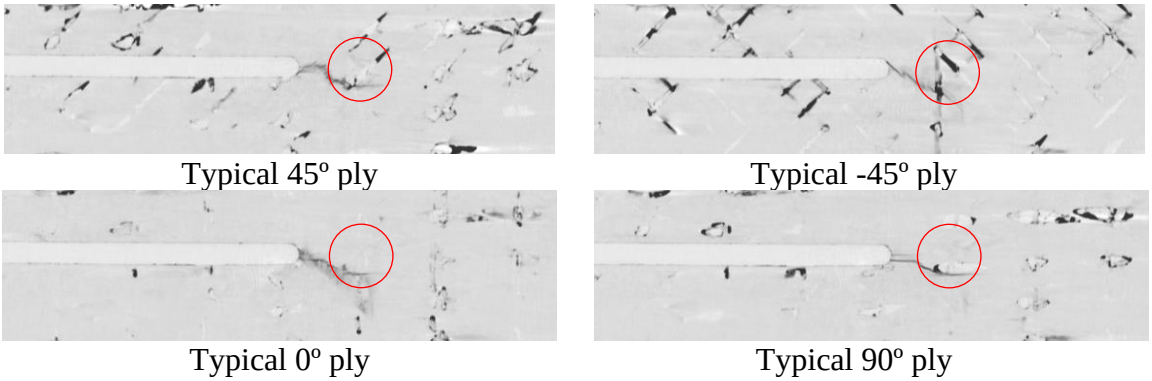

Figure 5. CT scan images of the damage process zone before the ultimate failure load from Test 4 showing self-similar crack propagation (a red circle with a 3-mm diameter indicating the damage process zone).

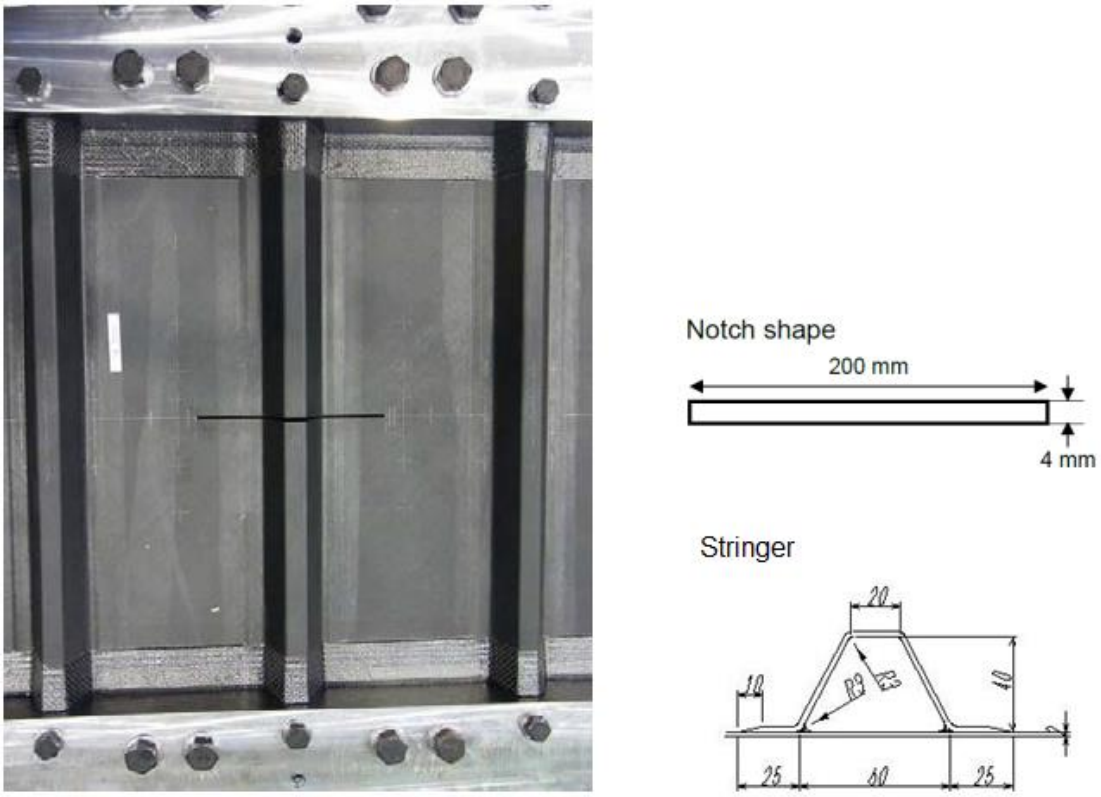

Figure 6. Full-scale stiffened panel tested at JAXA [2].

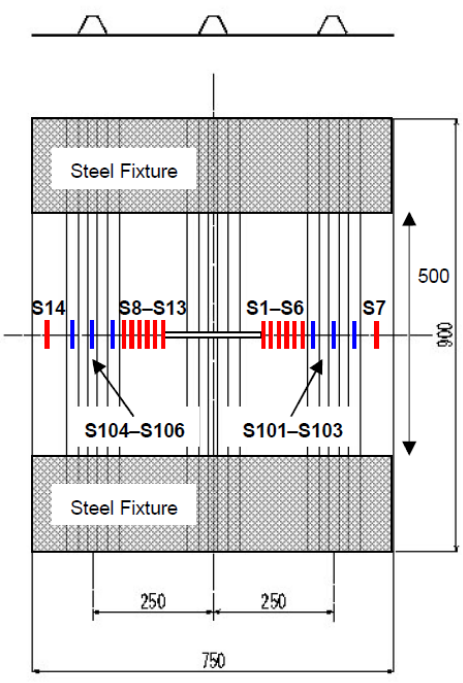

Gage No.	Location
S1(S8)	1.5 mm from notch tip
S2(S9)	5 mm from notch tip
S3(S10)	10 mm from notch tip
S4(S11)	20 mm from notch tip
S5(S12)	50 mm from notch tip
S6(S13)	80 mm from notch tip
S7(S14)	35mm from skin edge
S101 (S104)	On foot near to notch
S102(S105)	On top of stringer
S103(S106)	On foot far to notch

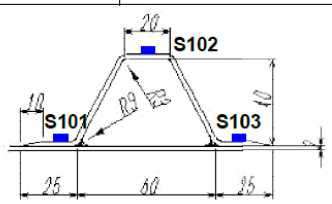

Figure 7. Location of strain gauges in the full-scale stiffened panel.

Specimen dimensions	Two notch lengths	
	Long-notch - 70 mm	Short-notch - 17.5 mm

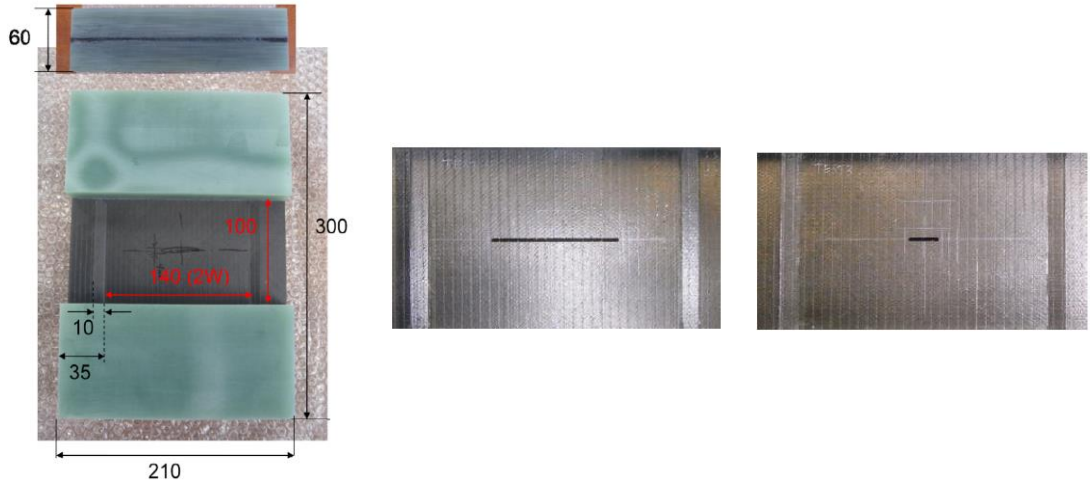

Figure 8. Scaled down coupons with two notch configurations.

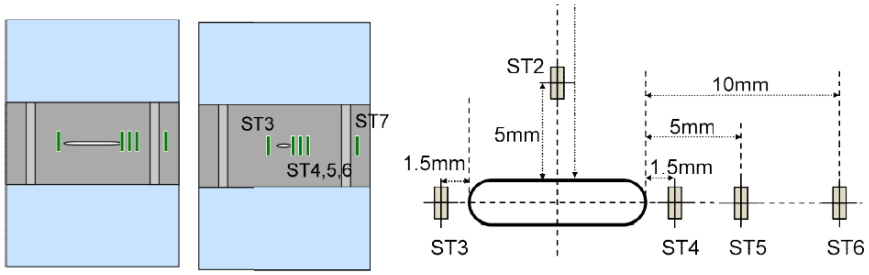

Figure 9. Location of the strain gauges in the small coupons.

Gage No.	Location
S1(S8)	1.5 mm from notch tip
S2(S9)	5 mm from notch tip
S3(S10)	10 mm from notch tip
S4(S11)	20 mm from notch tip
S5(S12)	50 mm from notch tip
S6(S13)	80 mm from notch tip
S7(S14)	35mm from skin edge

Strain gauge locations

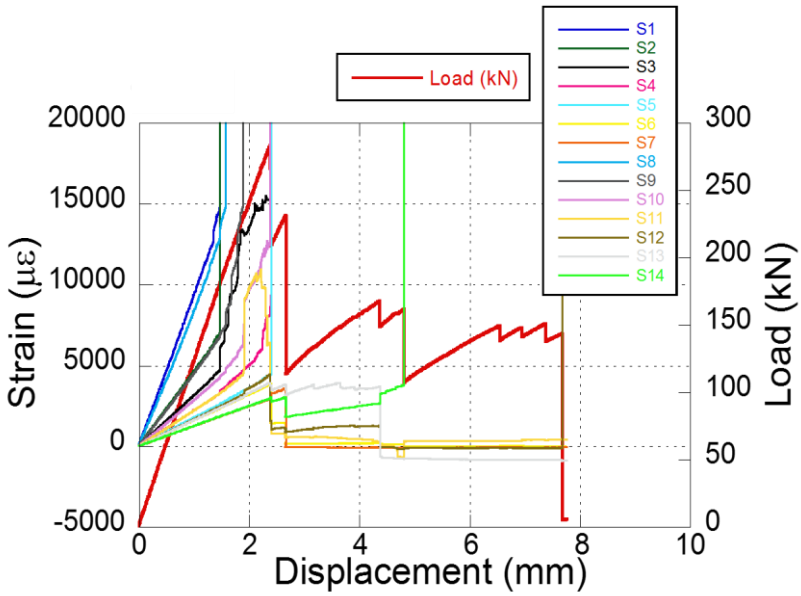

(a) Overall result

Gage No.	Location
S1(S8)	1.5 mm from notch tip
S2(S9)	5 mm from notch tip
S3(S10)	10 mm from notch tip
S4(S11)	20 mm from notch tip
S5(S12)	50 mm from notch tip
S6(S13)	80 mm from notch tip
S7(S14)	35mm from skin edge

Strain gauge locations

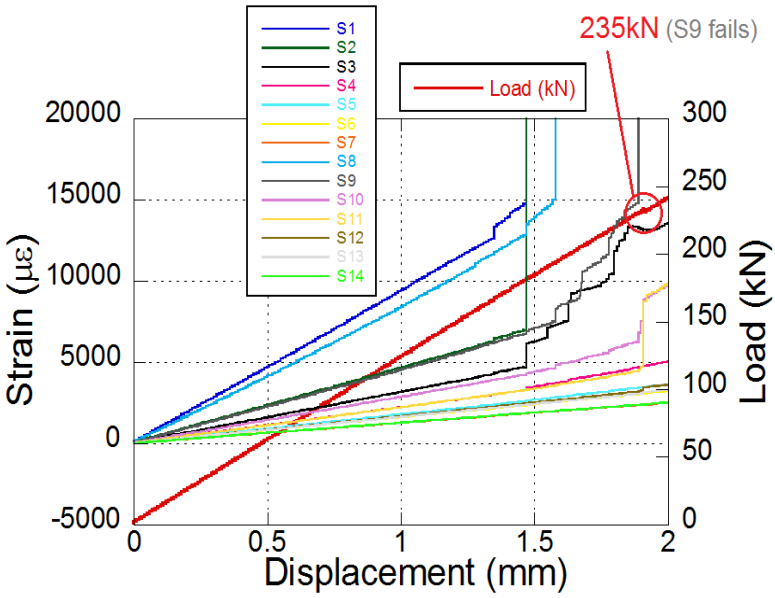

(b) Zoom-in view around initial fracture propagation

Figure 10. Experimental results of the full-scale stiffened panel test.

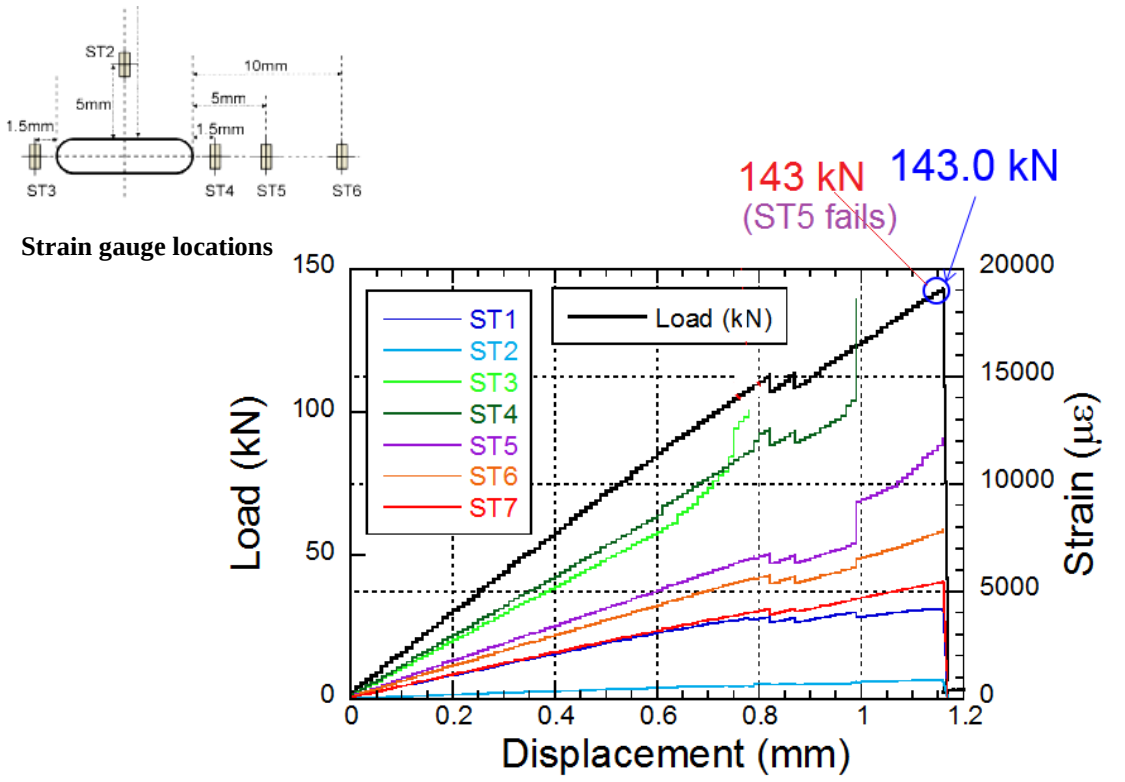

(a) Coupon with a short notch

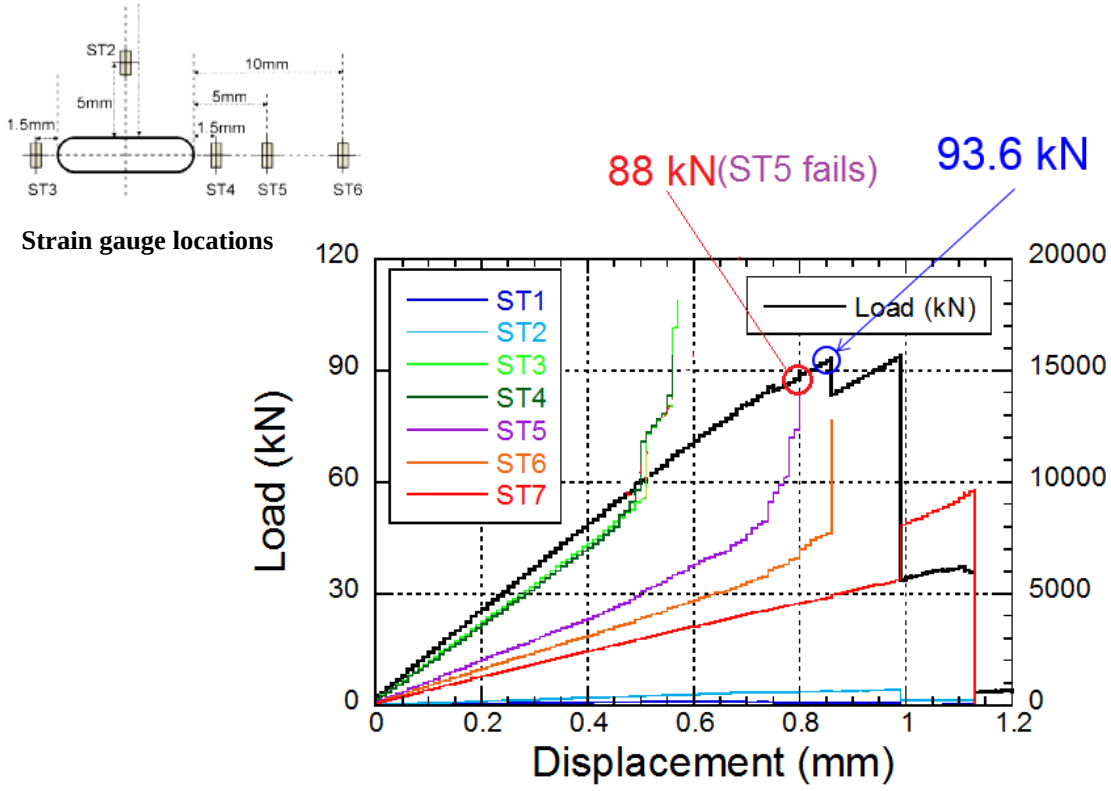

(b) Coupon with a long notch

Figure 11. Experimental results of stiffened coupon tests.

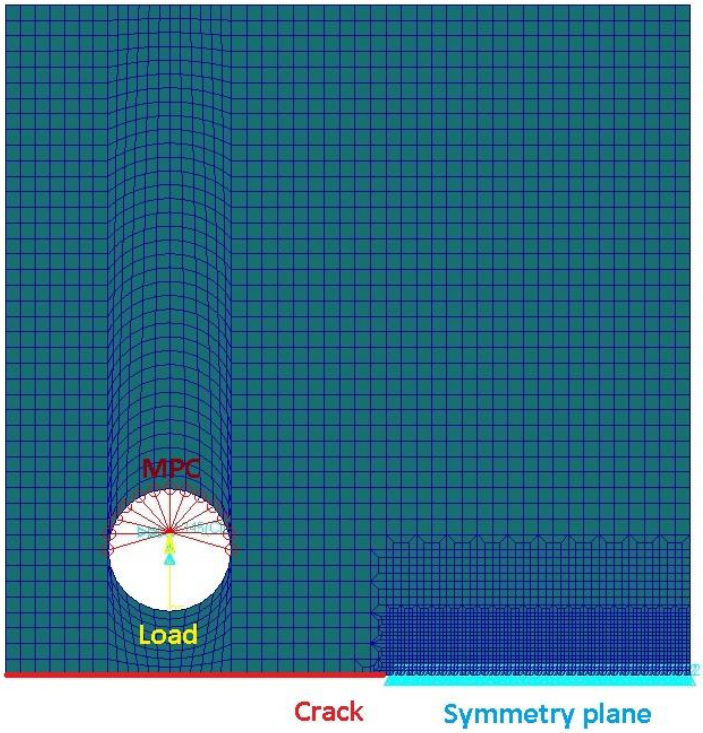

Figure 12. Applying VCCT to the scaled-down OCT specimen.

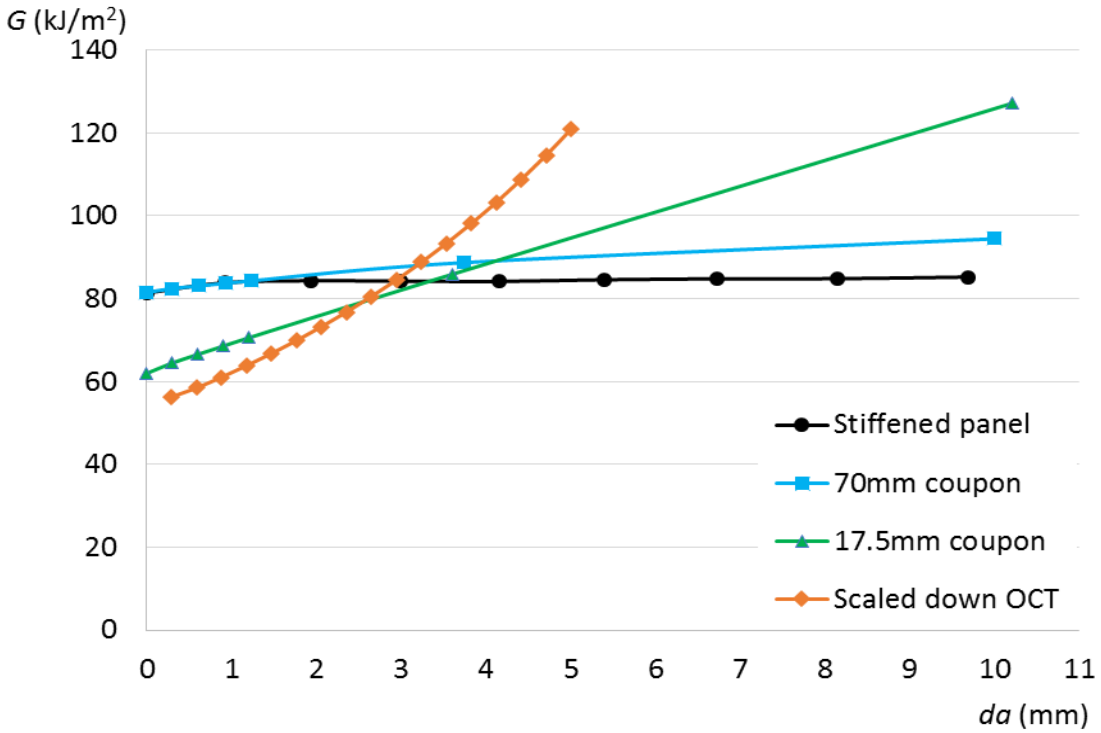

Figure 13. Calculated G-curves by taking loads at the failure of 5 mm strain gauges.

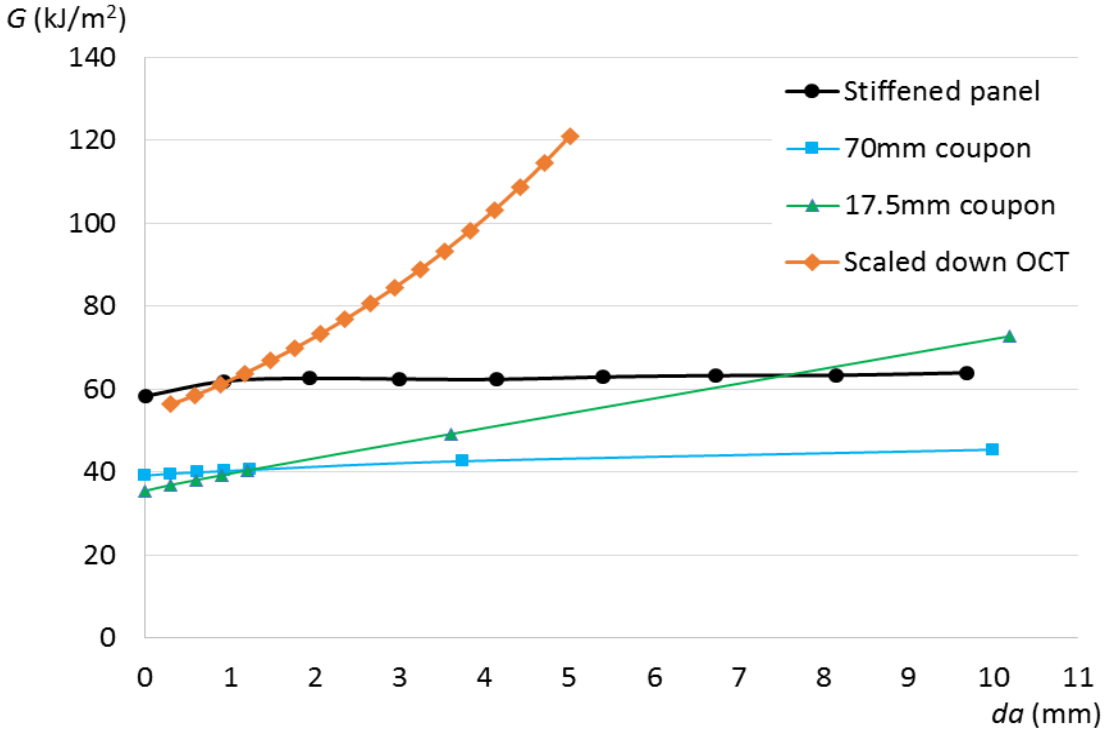

Figure 14. Calculated G-curves by taking loads at the failure of 1.5 mm strain gauges.

Table 1. Failure sequence of strain gauges in full-scale stiffened panel

Gauge number	Location	Gauge damage	Gauge failure[1]	Gauge unloading[2]
S1	1.5 mm	169 kN	182 kN	-
S8	1.5 mm	182 kN	197 kN	-
S2	5 mm	-	182 kN	-
S9	5 mm	197 kN	235 kN	-
S3	10 mm	182 kN	282 kN	-
S10	10 mm	235 kN	282 kN	-
S4	20 mm	263 kN	282 kN	-
S11	20 mm	235 kN	-	282 kN
S5	50 mm	-	282 kN	-
S12	50 mm		-	282 kN
S6	80 mm	-	-	282 kN
S13	80 mm	282 kN	-	168 kN
S7	Panel edge	-	-	231 kN
S14	Panel edge	-	162 kN	-

1. Strain gauge is on the crack path

2. Strain gauge is not on the crack path

Table 2. Material properties of solid elements for the laminates.

E **[GPa]**	***G*** **[GPa]**	***υ***
37.9	14.7	0.29